Elastodynamic Performance Evaluation and Comparison in Hydraulic and Electromechanical Linear Actuator Driven Heavy-Duty Manipulators

Aleksi Vesterinen, Goran R. Petrovic´ and Jouni Mattila

Faculty of Engineering and Natural Sciences, Tampere University, Finland,
aleksi.vesterinen@tuni.fi
Faculty of Engineering and Natural Sciences, Tampere University, Finland,
goran.petrovic@tuni.fi
Faculty of Engineering and Natural Sciences, Tampere University, Finland,
jouni.mattila@tuni.fi

Abstract

Strict global regulations and initiatives like Paris Agreement 2015 for achieving low carbon dioxide emission via energy efficiency nowadays have already made the electrification of hydraulic working machines and manipulators an actual topic, invested heavily into. During the first wave, diesel engine powered vehicles are being replaced with more-electric or all-electric battery electric vehicles (BEVs). Electrification is an emerging topic, and, for example, Doosan Bobcat has recently introduced an all-electric T7X model where diesel power is entirely replaced with BEV technology. Hydraulic linear actuators for the bucketare replaced with electromechanical linear actuators (EMLA) by Moog, and the main drive motors are also electric. These modern trends also require the development and broadening of the underlying structural and dynamics analysis when electric actuators are used instead of hydraulic ones. From the control perspective, natural frequencies provide insight into the manipulator dynamics and achievable performance depending on the current working point. Elastodynamic performance, which directly relates to the manipulator stiffness, is one of the most important performance indicators, especially when considering manipulator positioning. Methods for calculating manipulator natural frequencies are well known in the case of

hydraulic manipulators, where the effect of hydraulic fluid compressibility (causing spring effect) has been studied in detail. This paper, among others, provides means for calculating natural frequencies of oscillation in an electrified EMLA-driven manipulator, and expression for the equivalent of hydraulic spring behaviour is given. The natural frequencies are compared between the two manipulator versions, of which the hydraulic already exists, and the electric one is in the design process. In addition, the applicability of EMLAs is discussed with respect to current mobile hydraulic working machine requirements.

1 Introduction

In the process of manipulator design, the choice of physical properties, like manipulator lengths and masses, is usually a solution to some mechanism optimisation problem. Each optimisation problem contains a relevant cost function to be minimised or maximised considering certain kinematic and dynamic limitations in the process. Since optimal solutions in different optimisation tasks may be different in each separate case, it is critical to identify relevant performance indices and combine them appropriately. Identifying and choosing pertinent performance indices may not be an easy task since these can be conflicting. For example, decreasing the manipulator's inertia will decrease the stiffness of the manipulator; thus, inertia minimisation and stiffness maximisation are contradictory goals, among many others available.

Different performance indices proposed over the years cover many dynamic behaviour aspects. These can comprehend workspace size, velocity transmission, inertia, stiffness, and eigenfrequencies [1]. Jacobian matrix, manipulability, condition number, isotropy, and global conditioning indices are also to be considered per [2]. In addition, the inertia torque index and centrifugal torque index can be found as proposed in [3].

Among many available indices, the natural oscillation frequencies are appropriate performance measures that incorporate both kinematic and dynamic properties, relating directly to mechanical vibrations. The lowest natural oscillation frequency can be chosen as a design objective, aiming at minimising vibrations and avoiding the existence of directions with zero gain [4]. Even this isolated task *per se* is not trivial considering that natural frequencies (NF) change from posture to posture, thus having different values during the manipulator operation. Because of this, there will undoubtedly exist manipulator configurations that are more favourable than others from the aspect of induced vibrations.

When discussing already available manipulator solutions, it may be intriguing to gain insight into the distribution of NFs over the workspace if the manufacturer does not provide that information. In many cases, particularly when interacting with the surroundings, manipulator vibrations that affect, for example, the positioning accuracy or cause tool wear, can be induced. By having a clear insight into how NFs change over the workspace, unfavourable manipulator postures can be avoided in the operation process. In this case, mathematical models in the form of linearized equations of motion can serve as a handy primary tool for preliminary analysis.

Apart from providing a preliminary insight into the distribution of NFs, the elastodynamic modelling of manipulators forms a solid basis for the eventual parameter identification procedures. Natural oscillation frequencies can also be directly estimated from experimentally obtained frequency response plots without any prior analysis. The problem is that they can be determined experimentally only for selected configurations because verification in the whole workspace would require an infinite number of experiments. This topic has been addressed in papers [5] – [7], where measurements have been performed in many different, carefully selected robot configurations. NFs for a serial, six-degree-of-freedom (DOF) industrial robot with only rotational joints (6R) have been provided, along with experimental verifications of NFs using impulse response tests. Impulse responses in carefully chosen postures have been used in [8], followed by identifying joints' stiffness and damping. Elastodynamic modelling and parameter identification have also been researched in [9] – [10]. In the study [11], NF surfaces showing the distribution of six NFs are provided with analytic verifications in eight manipulator poses for a parallel manipulator. Beforehand obtained prediction of the lowest NF of a hydraulic manipulator, using CAD software, was used in the adaptive control algorithm [12]. Minimum natural oscillation frequencies are also shown to be an essential factor when designing robust linear controllers for hydraulic manipulators [13]. In mobile manipulators, the manipulator arm's minimum NF is important when designing arm controller [14].

The change of actuation means will undoubtedly affect elastodynamics performance and NF distribution in the manipulator. Ongoing mega-trends in non-road mobile machinery (NRMM) focus on reducing greenhouse gasses [15] and bring in front electric and hybrid prime movers. Continuing development of hybrid and all-electric solutions for electromechanical actuators [16] provides a possibility of having capable all-electric NRMM. Many global competitors have already released all-electric solutions with imminent heavy investing to follow. In all of these all-electric NRMM solutions, elec-

tromechanical linear actuators (EMLAs) play an essential role. Their effect and what the change of actuation paradigm brings, in general, should be investigated in detail.

The present study compares natural oscillation frequencies in a heavy-duty manipulator for two considered cases of importance. Analysing the oscillations caused by the hydraulic oil spring effect and when EMLA is retrofitted to the same manipulator, this paper provides insight into one of the governing and widely accepted dynamic performance indices. The presentation of an EMLA mathematical model is followed by a good overview of expected achievable manipulator performance if electrification was to be carried out. Plots showing the distribution of NFs over the workspace are shown for both cases accompanied with appropriate time responses and power spectre densities, which validate the carried out analysis.

By tackling the all-present topic of today - electrification of heavy-duty machinery, this study provides a guide to analysing the effects of electrification on the elastodynamic performance of heavy-duty manipulators.

2 Mathematical Modelling

2.1 Preliminaries

All the manipulator links in the following analysis will be considered rigid. Every rigid body in the analysis will have at least one three-dimensional coordinate system $\{\mathbf{A}\}$ (called frame $\{\mathbf{A}\}$ in the following text) attached to it.

Let the linear and angular velocities as would be sensed in frame $\{\mathbf{A}\}$ be denoted throughout the paper as ${}^{\mathbf{A}}v = \begin{pmatrix} {}^{\mathbf{A}}v_{\mathrm{x}} & {}^{\mathbf{A}}v_{\mathrm{y}} & {}^{\mathbf{A}}v_{\mathrm{z}} \end{pmatrix}^T \in \mathbb{R}^{3\times 1}$ and ${}^{\mathbf{A}}\omega = \begin{pmatrix} {}^{\mathbf{A}}\omega_{\mathrm{x}} & {}^{\mathbf{A}}\omega_{\mathrm{y}} & {}^{\mathbf{A}}\omega_{\mathrm{z}} \end{pmatrix}^T \in \mathbb{R}^{3\times 1}$, respectively. The set of independent generalized coordinates represents the minimal number of geometric parameters which can be used to uniquely describe the motion of a mechanical system. In the following considerations the vector of generalized coordinates will be:

$$\xi = (\xi_1 \quad \xi_2 \quad \dots \quad \xi_i \quad \dots \quad \xi_n)^T \in \mathbb{R}^{n\times 1}, \tag{1}$$

and the corresponding generalized force vector will be:

$$\tau(\dot{\xi},\xi) = \left(\tau_1(\dot{\xi},\xi)\dots\tau_i(\dot{\xi},\xi)\dots\tau_n(\dot{\xi},\xi)\right)^T \in \mathbb{R}^{n\times 1}. \tag{2}$$

2.2 Choosing the Modelling Formalism

Different approaches for mathematical modelling of manipulator dynamics lead to different sets of equations, each having both specific advantages and downsides. Full-dynamics modelling of serial-parallel manipulators with little or no approximations, including the linear actuator masses and accounting for closed-loop kinematics relations, has been provided using the Lagrange formalism **MC**, in the Newton-Euler framework [17] and using Kane's equations obtained combining screw theory and the principle of virtual work [18].

The Lagrange approach based on kinetic and potential energies and the Newton-Euler approach based on the balance of all the forces acting on a rigid body is considered the most popular. The Newton-Euler approach is considered more fundamental and computationally efficient, [19]. With its very effective, recursive formulation, it enables subsystem-by-subsystem analysis and thus is indispensable in the VDC framework where the control action is formed on the subsystem level to guarantee the stability of the whole system [20]. It is also the most natural approach when reaction forces are included in the analysis [21]. The RNEA will effectively provide the identical inverse and direct dynamics calculations results as other methods would, but it will not lead directly to the most convenient form when performing the elastodynamic performance assessment. Except in simple cases, there will be more equations than degrees of freedom with RNEA. A potentially tedious procedure of combining equations might be needed when starting from RNEA to arrive at the manipulator dynamics description in the joint-space with the number of equations equalling the number of generalised coordinates. Formulating a system of linear equations like this is essential since it serves as the starting point in the elastodynamics performance analysis. The Lagrange approach leads directly to the same number of equations as is the number of generalised coordinates. These equations may be pretty complex, which is significantly magnified in the presence of the closed kinematic loops where the expressions for derivatives of the loop-closure function per generalised coordinates will usually introduce additional complexity. Still, their linearization results give the most direct path to the equations required in the considered context here, and thus, the dynamics of the manipulator analyzed here will be modelled using the Lagrange equations of the second kind. In the presented study, masses of linear actuator in rotational segments will be neglected when forming equations of motions since it will simplify the anal-

ysis and not reflect significantly on the elastodynamic performance analysis for the considered manipulator configuration with its underlying properties.

2.3 Equations of Motion

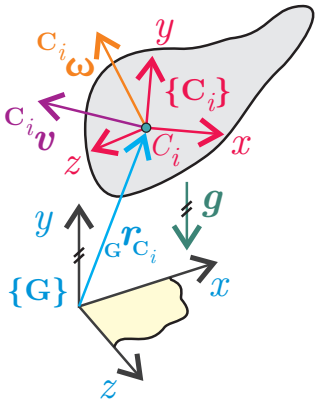

Figure 1 Considered rigid body.

Let us observe the i-th rigid body from Fig. 1, belonging to a multibody system. Kinetic energy of the i-th rigid body, labelled as $K_i(\dot{\xi},\xi) \in \mathbb{R}$, is per definition:

$$K_i(\dot{\xi},\xi) = \frac{1}{2} m_i v_{C_i}^T v_{C_i} + \frac{1}{2} {}^{\mathbf{C}_i}\boldsymbol{\omega}^T \left[{}^{\mathbf{C}_i}\mathbf{I}\right] {}^{\mathbf{C}_i}\boldsymbol{\omega}, \tag{3}$$

with $m_i \in \mathbb{R}$ being the body mass, $v_{C_i} \in \mathbb{R}^{3\times 1}$ is the considered COM velocity vector with respect to the inertial frame $\{\mathbf{G}\}$ and expressed in any convenient frame, $\left[{}^{\mathbf{C}_i}\mathbf{I}\right] \in \mathbb{R}^{3\times 3}$ denotes the tensor of inertia of the i-th rigid body about the axes of the $\{\mathbf{C}_i\}$ frame with its origin the the centre of mass (COM) C_i. Assuming that the gravity acceleration is constant and normal to the Earth-tangent plane Oxz, one way to define the potential energy $\Pi_i(\xi) \in \mathbb{R}$ of the considered i-th body is:

$$\Pi_i(\xi) = m_i g\, y_{C_i}(\xi), \tag{4}$$

where $g \in \mathbb{R}$ denotes the gravity acceleration magnitude and $y_{C_i}(\xi) \in \mathbb{R}$ denotes the y-coordinate value of the i-th rigid body COM with respect to the inertial frame $\{\mathbf{G}\}$, expressed in the $\{\mathbf{G}\}$ frame. If the Lagrange function is introduced by definition as the sum of difference between the kinetic and

potential energy of the whole rigid body system, which is composed of n rigid bodies, as:

$$\mathcal{L}(\dot{\xi},\xi) = \sum_{i=1}^{n} \left(K_i(\dot{\xi},\xi) - \Pi_i(\xi) \right), \tag{5}$$

then Lagrange equations of the second kind for a rigid body system can be written in the form of a system:

$$\frac{\mathrm{d}}{\mathrm{d}t}\left(\frac{\partial \mathcal{L}(\dot{\xi},\xi)}{\partial \dot{\xi}^i} \right) - \frac{\partial \mathcal{L}(\dot{\xi},\xi)}{\partial \xi^i} = \tau_i(\dot{\xi},\xi), \quad i = 1,...,n, \tag{6}$$

where $\tau_i(\dot{\xi},\xi) \in \mathbb{R}$ here denotes the generalized forces arising as the consequence of all the other forces acting upon the system, apart from the weight force which is comprehended through the potential energy. In the analyzed case, the generalized forces analysis will play an important role and will be addressed in more detail.

System of equations (6) can be rearranged and written in the form that is widely used:

$$\mathbf{M}(\xi)\,\ddot{\xi} + \mathbf{C}\left(\dot{\xi},\xi\right)\dot{\xi} + \mathbf{G}(\xi) = \tau\left(\dot{\xi},\xi\right), \tag{7}$$

with $\mathbf{M}(\xi) \in \mathbb{R}^{n\times n}$, denoting the real, symmetric and positive-definite mass matrix, $\mathbf{C}\left(\dot{\xi},\xi\right) \in \mathbb{R}^{n\times n}$ being the Coriolis/centrifugal matrix and $\mathbf{G}(\xi) \in \mathbb{R}^{n\times 1}$ representing the vector of gravity-related terms.

2.4 Linearized EOM and elastodynamic performance

Linearizing the equations of motion about the nominal manipulator posture in the resting state, determined with $\left(\dot{\xi},\xi\right) = (\mathbf{0},\xi_0)$ returns the system of linear ODEs:

$$\mathbf{E}_0(\xi_0)\,\Delta\ddot{\xi} + \mathbf{H}_0(\xi_0)\,\Delta\xi = \Delta\tau. \tag{8}$$

Assuming that generalized force perturbation term $\Delta\tau$ can be represented here in the general case as:

$$\Delta\tau = -\mathbf{F}_0(\xi_0)\,\Delta\dot{\xi} - \mathbf{K}_0(\xi_0)\,\Delta\xi, \tag{9}$$

leads to the common linearized form:

$$\mathbf{E}_0\,\Delta\ddot{\xi} + \mathbf{F}_0\,\Delta\dot{\xi} + (\mathbf{H}_0 + \mathbf{K}_0)\,\Delta\xi = 0, \tag{10}$$

where the matrix $\mathbf{E}_0(\xi_0)$ can be directly obtained from the mass matrix as:

$$\mathbf{E}_0(\xi_0) = \mathbf{M}(\xi_0), \tag{11}$$

matrix $\mathbf{F}_0(\xi_0)$ will be a consequence of dissipative friction forces and matrix $\mathbf{K}_0(\xi_0)$ will comprehend spring-like behaviour of linear actuators being considered here.

After choosing the state variables vector as:

$$\mathbf{x} = \left(\Delta\xi, \Delta\dot{\xi}\right)^T \in \mathbb{R}^{2n\times 1} \tag{12}$$

the system of equations from Eq. (10) can be rewritten as:

$$\dot{\mathbf{x}} = \mathbf{A}\left(\xi_0\right)\mathbf{x}, \tag{13}$$

with matrix $\mathbf{A}\left(\xi_0\right) \in \mathbb{R}^{2n\times 2n}$ being defined as:

$$\mathbf{A}\left(\xi_0\right) = \begin{pmatrix} \mathbf{O}_{n\times n} & \mathbf{I}_{n\times n} \\ -\mathbf{E}_0^{-1}\left(\mathbf{H}_0 + \mathbf{K}_0\right) & -\mathbf{E}_0^{-1}\mathbf{F}_0 \end{pmatrix}. \tag{14}$$

Eigenvalues and eigenvectors of matrix $\mathbf{A}\left(\xi_0\right)$ will determine the properties of unforced vibrations in the system, [22]. In the present study it is of interest to investigate how frequencies of unforced oscillations change when hydraulic linear actuators are replaced with electric counterparts. Thus, magnitudes of matrix $\mathbf{A}\left(\xi_0\right)$ eigenvalues will be investigated.

3 Spring-like Behaviour of Linear Actuators

While the matrices $\mathbf{E}_0(\xi_0)$ and $\mathbf{H}_0(\xi_0)$ from (10) can be fully determined by knowing the kinematic and mass properties of the considered manipulator, matrices $\mathbf{F}_0(\xi_0)$ and $\mathbf{K}_0(\xi_0)$ from (9) depend on the actuation type and actuator properties. In hydraulic systems at zero flow, and electromechanical systems, at nominal holding force/torque, motions exist due to the spring-like behaviour of the actuator.

3.1 Hydraulic Spring Effect

The effect of oil compressibility is known to cause the existence of "hydraulic spring" [23]. The existence of free oscillations can be attributed to the spring-like behaviour of the oil in cylinder chambers where the spring stiffness is varying.

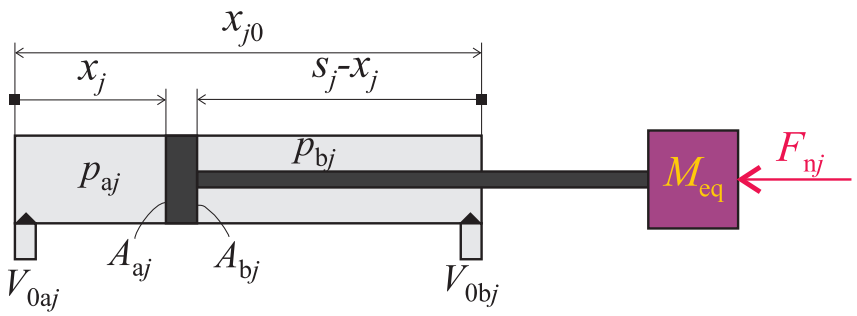

Figure 2 Linear hydraulic actuator.

Let us observe the j-th linear hydraulic actuator in Fig. 2. The linear momentum change of moving parts is:

$$M_{\mathrm{eq}j}\ddot{x}_j + C_{\mathrm{eq}j}\dot{x}_j = p_{\mathrm{a}j}A_{\mathrm{a}j} - p_{\mathrm{b}j}A_{\mathrm{b}j} - F_{\mathrm{n}j}, \tag{15}$$

where $M_{\mathrm{eq}j}$ is the equivalent mass of moving parts, $C_{\mathrm{eq}j}$ is the viscous damping coefficient and $F_{\mathrm{n}j}$ is the external force. Chamber pressures p_{aj} and p_{bj} create the actuation force by acting on piston areas A_{aj} and A_{bj}. At zero flows to both chambers, the pressures change as follows:

$$\dot{p}_{\mathrm{a}j} = -\frac{B_{\mathrm{a}j}A_{\mathrm{a}j}}{V_{0\mathrm{a}j} + A_{\mathrm{a}j}x_j}\dot{x}_j, \tag{16}$$

and:

$$\dot{p}_{\mathrm{b}j} = -\frac{B_{\mathrm{b}j}A_{\mathrm{b}j}}{V_{0\mathrm{b}j} + A_{\mathrm{b}j}\,(s_j - x_j)}\dot{x}_j, \tag{17}$$

with $B_{\mathrm{a}j}$ and $B_{\mathrm{b}j}$ representing the hydraulic fluid bulk moduli, and where the fluid volumes in hoses between the j-th direction valve and actuator chambers are $V_{0\mathrm{a}j}$ and $V_{0\mathrm{b}j}$.

Combining (15) – (17) one can arrive at the equation describing the motion of moving parts at zero flows as:

$$M_{\mathrm{eq}j}\dddot{x}_j + C_{\mathrm{eq}j}\ddot{x}_j + K_{\mathrm{hs}j}\dot{x}_j = -\dot{F}_{\mathrm{n}j}. \tag{18}$$

Once (18) is linearized about the equilibrium position determined with the piston position $x_{j\mathrm{N}}$, an equation describing motion in the vicinity of the nominal equilibrium point is:

$$M_{\mathrm{eq}j}\Delta\ddot{x}_j + C_{\mathrm{eq}j}\Delta\dot{x}_j + K_{\mathrm{hs}j\mathrm{N}}\Delta x_j = -\Delta F_{\mathrm{n}j}, \tag{19}$$

where the hydraulic spring stiffness $K_{\mathrm{hs}jN}$ is:

$$K_{\mathrm{hs}jN} = \frac{B_{\mathrm{a}j} A_{\mathrm{a}j}^2}{V_{0\mathrm{a}j} + A_{\mathrm{a}j}\, x_{jN}} + \frac{B_{\mathrm{b}j} A_{\mathrm{b}j}^2}{V_{0\mathrm{b}j} + A_{\mathrm{b}j}\,(s_j - x_{jN})}, \tag{20}$$

and the equivalent actuator stiffness $K_{\mathrm{h}j}$ is calculated from:

$$\frac{1}{K_{\mathrm{h}j}} = \frac{1}{K_{\mathrm{hs}jN}} + \frac{1}{K_{\mathrm{r}j}}, \tag{21}$$

with $K_{\mathrm{r}j}$ representing the j-th actuator rod stiffness.

3.2 Equivalent Spring Stiffness in EMLAs

Different mathematical models of EMLAs have been proposed over many years of extensive research [24] – [25]. They differ in form, complexity and methodology used. It is argued and shown through experiments that, as expected, higher-order models better capture the dynamic behaviour and predict the resonant peaks. Since the near-steady state behaviour is contemplated in the presented study, an adapted fourth-order model from [26] will be used, since it suffices for the overall picture that is to be presented here.

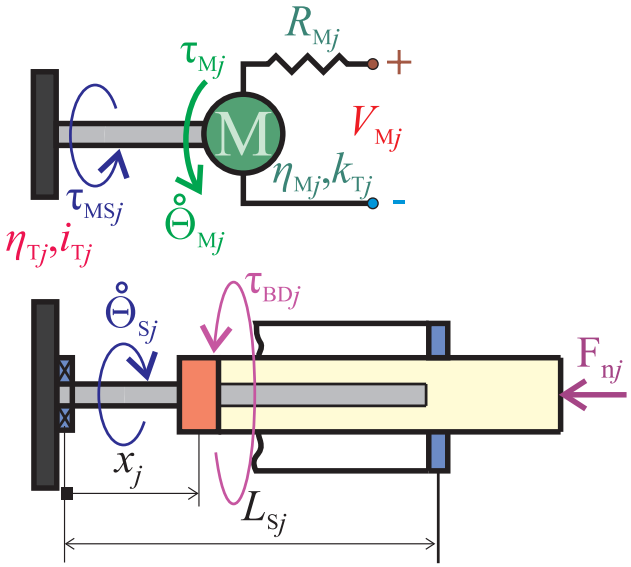

Figure 3 Schematic of an EMLA.

Let us observe the simplified schematics of an EMLA actuated with a DC motor in Fig. 3 and let us incorporate some of the modelling ideas from [27] for the sake of obtaining an insightful nonlinear model. If the inductivity of motor coils is neglected, the current flow $I_{\mathrm{M}j}$ in the windings of j-th EMLA can be approximately determined as follows:

$$V_{\mathrm{M}j} - k_{\mathrm{M}j}\,\dot{\Theta}_{\mathrm{M}j} = R_{\mathrm{M}j}\,I_{\mathrm{M}j}, \tag{22}$$

where $R_{\mathrm{M}j}$ is the resistance of coils, $V_{\mathrm{M}j}$ is the applied voltage, $\dot{\Theta}_{\mathrm{M}j}$ represents the motor shaft angular velocity, and $k_{\mathrm{M}j}$ is the back-electromotive force coefficient. The angular momentum change of the j-th DC motor shaft is:

$$J_{\mathrm{M}j}\,\ddot{\Theta}_{\mathrm{M}j} + C_{\mathrm{M}j}\,\dot{\Theta}_{\mathrm{M}j} + \tau_{\mathrm{MS}j} = \tau_{\mathrm{M}j}, \tag{23}$$

where $J_{\mathrm{M}j}$ represents the moment of inertia of motor rotating parts and motor shaft, $C_{\mathrm{M}j}$ is the viscous damping coefficient, $\tau_{\mathrm{MS}j}$ is the part of the motor actuation moment that is transferred to the load shaft. The j-th DC motor actuation moment $\tau_{\mathrm{M}j}$ can be calculated from:

$$\tau_{\mathrm{M}j} = \eta_{\mathrm{M}j}\,k_{\mathrm{T}j}\,I_{\mathrm{M}j}, \tag{24}$$

as a function of motor efficiency $\eta_{\mathrm{M}j}$ and torque constant $k_{\mathrm{T}j}$.

The transmission ratio $i_{\mathrm{T}j}$ relates angular velocities as:

$$\dot{\Theta}_{\mathrm{S}j}\,i_{\mathrm{T}j} = \dot{\Theta}_{\mathrm{M}j}, \tag{25}$$

where $\dot{\Theta}_{\mathrm{S}j}$ is the j-th EMLA shaft angular velocity.

Because it will be convenient to express certain following relations in terms of linear nut displacement $x_{\mathrm{n}j}$, the nut linear velocity $\dot{x}_{\mathrm{n}j}$ is related with load shaft angular velocity as:

$$\dot{x}_{\mathrm{n}j} = \frac{p_j}{2\pi}\,\dot{\Theta}_{\mathrm{S}j}, \tag{26}$$

where p_j is the j-th ballscrew pitch.

The load shaft rotates per relation similar to (23):

$$J_{\mathrm{S}j}\,\ddot{\Theta}_{\mathrm{S}j} + C_{\mathrm{S}j}\,\dot{\Theta}_{\mathrm{S}j} = i_{\mathrm{T}j}\,\tau_{\mathrm{MS}j} - \tau_{\mathrm{BD}j}, \tag{27}$$

where again as before, $J_{\mathrm{S}j}$ represents the moment of inertia of rotating parts on the load shaft, $C_{\mathrm{S}j}$ is the viscous damping coefficient, and $\tau_{\mathrm{BD}j}$ is the ballscrew back-drive moment:

$$\tau_{\mathrm{BD}j} = \frac{p_j}{2\pi}\left(C_{\mathrm{BS}j}\left(\dot{x}_{\mathrm{n}j} - \dot{x}_j\right) + K_{\mathrm{BS}j}\left(x_{\mathrm{n}j} - x_j\right)\right), \tag{28}$$

with the ballscrew equivalent stiffness $K_{\mathrm{BS}j}$, $C_{\mathrm{BS}j}$ denotes ballscrew damping coefficient, $\dot{x}_j$ and x_j are the velocity and position of the EMLA rod, respectively.

Combining equations (22)–(28), one can arrive at:

$$J_j^* \ddot{x}_{\mathrm{n}j} + C_j^* \dot{x}_{\mathrm{n}j} + C_{\mathrm{BS}j}(\dot{x}_{\mathrm{n}j} - \dot{x}_j) + K_{\mathrm{BS}j}(x_{\mathrm{n}j} - x_j) = K_j^* V_{\mathrm{M}j}, \tag{29}$$

where:

$$J_j^* = \left(J_{\mathrm{M}j} i_{\mathrm{T}j}^2 + J_{\mathrm{S}j}\right) \left(\frac{2\pi}{p_j}\right)^2, \tag{30}$$

$$C_j^* = \left(C_{\mathrm{M}j} i_{\mathrm{T}j}^2 + C_{\mathrm{S}j}\right) \left(\frac{2\pi}{p_j}\right)^2, \tag{31}$$

$$K_j^* = \frac{k_{\mathrm{T}j}\,\eta_{\mathrm{M}j}}{R_{\mathrm{M}j}} \frac{2\pi}{p_j}. \tag{32}$$

The motion of linearly moving EMLA parts follows:

$$M_j \ddot{x}_j + C_j \dot{x}_j + C_{\mathrm{BS}j}(\dot{x}_j - \dot{x}_{\mathrm{n}j}) + K_{\mathrm{BS}j}(x_j)(x_j - x_{\mathrm{n}j}) = -F_{\mathrm{n}j}. \tag{33}$$

Equivalent EMLA stiffness $K_{\mathrm{BS}j}(x_j)$ plays a cruicual role in determining NFs of a manipulator with EMLAs. This equivalent ballscrew stiffness of the j-th ballscrew is:

$$K_{\mathrm{BS}j} = \left(\frac{x_j}{K_{\mathrm{s}j}} + \frac{1}{K_{\mathrm{b}j}} + \frac{1}{K_{\mathrm{n}j}} + \frac{1}{K_{\mathrm{r}j}} + \frac{p^2 x_j}{4K_{\mathrm{rot}j}\pi^2}\right)^{-1} \tag{34}$$

if the EMLA shaft is fixed on one side, or:

$$K_{\mathrm{BS}j} = \left(\frac{L_{\mathrm{eff}j}}{K_{\mathrm{s}j}} + \frac{1}{2K_{\mathrm{b}j}} + \frac{1}{K_{\mathrm{n}j}} + \frac{1}{K_{\mathrm{r}j}} + \frac{p^2 x_j}{4K_{\mathrm{rot}j}\pi^2}\right)^{-1} \tag{35}$$

when the EMLA shaft is fixed on both sides. In both (34) and (35) term $K_{\mathrm{s}j}$ represents the axial stiffness of the j-th EMLA shaft, $K_{\mathrm{b}j}$ represents the bearing stiffness, $K_{\mathrm{n}j}$ stands for the stiffness of the nut, $K_{\mathrm{r}j}$ is the stiffness of the rod, and $K_{\mathrm{rot}j}$ is the rotational stiffness of the shaft. Term $L_{\mathrm{eff}j}$ is related to the effective length of the shaft and it can be calculated as:

$$L_{\mathrm{eff}j} = \left(\frac{x_j(L_{\mathrm{S}j} - x_j)}{L_{\mathrm{S}j}}\right), \tag{36}$$

where L_{Sj} is the distance between the bearings.

While (29) and (33) represent the governing nonlinear EMLA equations, their linearized versions will be investigated as was the case with hydraulic actuator. Choosing the state variables as deviations from the equilibrium:

$$\Delta x_{\mathrm{E}} = \begin{pmatrix} \Delta x_{\mathrm{n}j} \\ \Delta x_j \end{pmatrix}, \tag{37}$$

equations (29) and (33) can be linearized and written as:

$$\mathbf{M}_{\mathrm{E}j}\,\Delta\ddot{x}_{\mathrm{E}j} + \mathbf{C}_{\mathrm{E}j}\,\Delta\dot{x}_{\mathrm{E}j} + \mathbf{K}_{\mathrm{BS}j}\,\Delta x_{\mathrm{E}j} = \Delta\mathbf{u}_{\mathrm{E}j}, \tag{38}$$

where appropriate system matrices are:

$$\mathbf{M}_{\mathrm{E}j} = \begin{pmatrix} J_j^* & 0 \\ 0 & M_j \end{pmatrix}, \tag{39}$$

$$\mathbf{C}_{\mathrm{E}j} = \begin{pmatrix} C_j^* + C_{\mathrm{BS}j} & -C_{\mathrm{BS}j} \\ -C_{\mathrm{BS}j} & C_{\mathrm{BS}j} + C_j \end{pmatrix}, \tag{40}$$

$$\mathbf{K}_{\mathrm{BS}j} = \begin{pmatrix} K_{\mathrm{BS}j\mathrm{N}} & -K'_{\mathrm{BS}j\mathrm{N}}\,x_{j\mathrm{N}} - K_{\mathrm{BS}j\mathrm{N}} \\ -K_{\mathrm{BS}j\mathrm{N}} & K'_{\mathrm{BS}j\mathrm{N}}\,x_{j\mathrm{N}} + K_{\mathrm{BS}j\mathrm{N}} \end{pmatrix}, \tag{41}$$

and:

$$\Delta\mathbf{u}_{\mathrm{E}j} = \begin{pmatrix} K_j^*\,\Delta V_{\mathrm{M}j} \\ -\Delta F_{nj} \end{pmatrix}. \tag{42}$$

Considering the expected magnitudes of coefficients, an equivalent EMLA spring value calculated from (34) or (35) as $K_{\mathrm{BS}j\mathrm{N}} = K_{\mathrm{BS}j}(x_{j\mathrm{N}})$ can be used when addressing the effect of EMLA on the distribution of NFs over the workspace.

3.3 Linearized Force Moments in Revolute Joints

The equivalent spring stiffness is essential to calculate the spring-like force that an actuator produces when small-amplitude oscillations about the equilibrium are analyzed. These forces should be related to the angular motion exhibited by revolute joints as a final step.

Let us observe revolute joint actuated with linear actuator, shown in Fig. 4. For small angle displacements $\Delta\xi_j$, spring-like force is generated in the actuator per:

$$\Delta F_j = -k_j\,\Delta x_j = -k_j\,L_{\tau j}\,\Delta\xi_j, \tag{43}$$

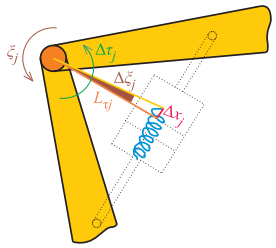

Figure 4 i-th revolute joint in a manipulator arm.

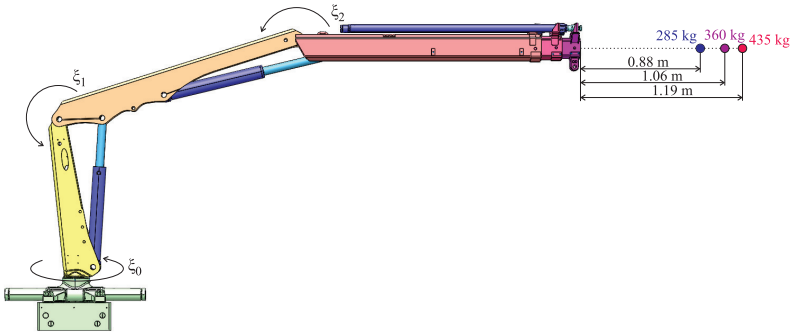

Figure 5 Considered manipulator arm, shown with linear hydraulic manipulators. Alongside are shown COMs of three different loads for which the analytic results are provided.

which after multiplying with the moment arm $L_{\tau j}$ gives the moment acting on the joint as:

$$\Delta\tau_j = -k_j L_{\tau j}^2 \Delta\xi_j. \tag{44}$$

In the case of prismatic joints, the modelling task is rather trivial, requiring just the force increment:

$$\Delta F_j = -k_j \Delta x_j. \tag{45}$$

Thus, the matrix $\mathbf{K}_0(\xi)$ has the following description:

$$\mathbf{K}_0(\xi) = \mathrm{diag}(k_{11}(\xi_1)\dots k_{ii}(\xi_i)\dots k_{nn}(\xi_n)), \tag{46}$$

where:

$$k_{ii} = \begin{cases} k_j & \text{if the joint is prismatic,} \\ k_j L_{\tau j}^2 & \text{if the joint is revolute.} \end{cases} \tag{47}$$

By modelling the friction as a locally linear function of velocity, matrix $\mathbf{F}_0$ can be written as:

$$\mathbf{F}_0 = \mathrm{diag}(f_{11}(\xi_1)\dots f_{ii}(\xi_i)\dots f_{nn}(\xi_n)), \tag{48}$$

with f_{ii} being a constant.

4 Comparing Distributions of Natural Oscillation Frequencies

Let us now analyze the heavy-duty manipulator from Fig. 5 based on the approaches described above. The effect of three different loads with different locations for their respective COMs will be investigated. Appropriate NF surfaces will be given for these three cases that can also be seen illustrated in Fig. 5 along with appropriate numeric values. Three generalized coordinates ξ_0, ξ_1, and ξ_2 will be used in the NF analysis. Although the base actuator stiffness will have different values as ξ_0 varies, the presented surfaces are provided for $\xi_0 = 0$. This suffices for the comparison needs.

Figures 6 - 8 show the distribution of $\omega_i, i = 0,1,2$ NFs in the case of hydraulic actuation over the $\xi_1 - \xi_2$ plane.

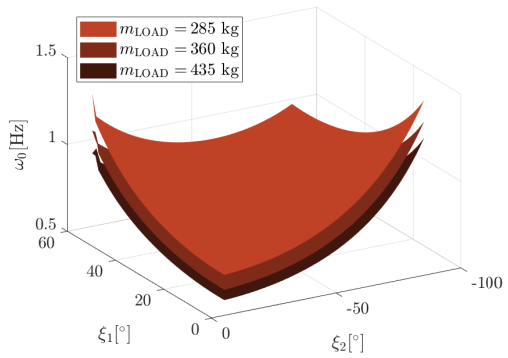

Figure 6 NF ω_0 distribution over the $\xi_1 - \xi_2$ plane (hydraulics).

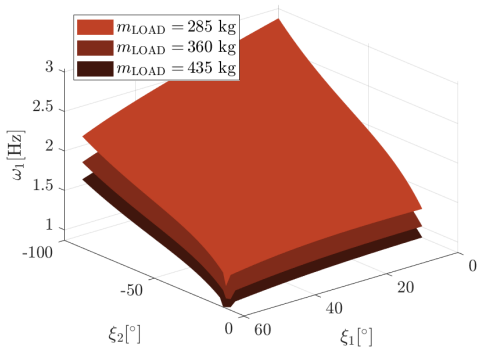

Figure 7 NF ω_1 distribution over the $\xi_1 - \xi_2$ plane (hydraulics).

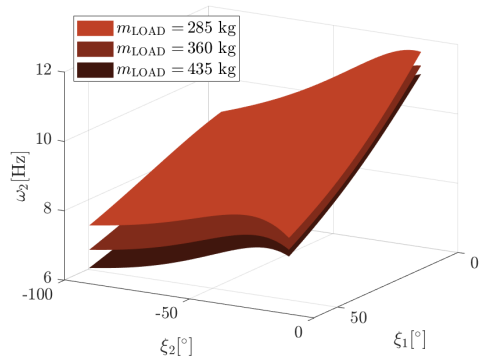

Figure 8 NF ω_2 distribution over the $\xi_1 - \xi_2$ plane (hydraulics).

Base rotation EMLA is designed such that two fixed supports restrain its motion, and the equivalent stiffness is calculated per (35). For EMLAs in the lift and tilt joint, the equivalent stiffness is calculated using (34). Figures 9 - 11 show the distribution of NFs in the case of electric actuation.

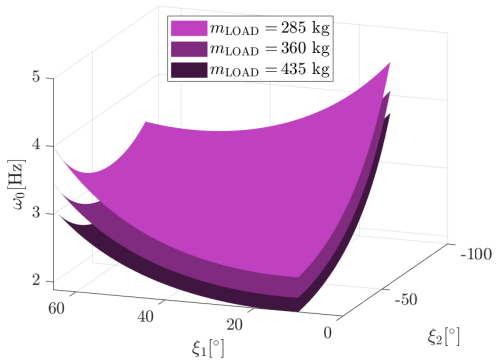

Figure 9 NF ω_0 distribution over the $\xi_1 - \xi_2$ plane (EMLA).

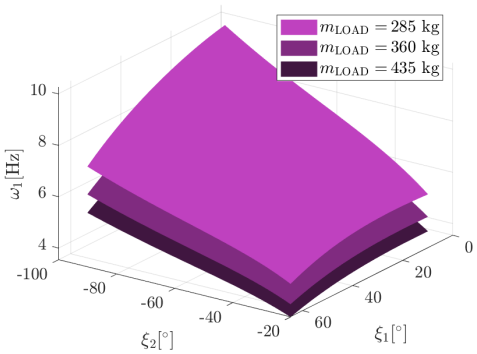

Figure 10 NF ω_1 distribution over the $\xi_1 - \xi_2$ plane (EMLA).

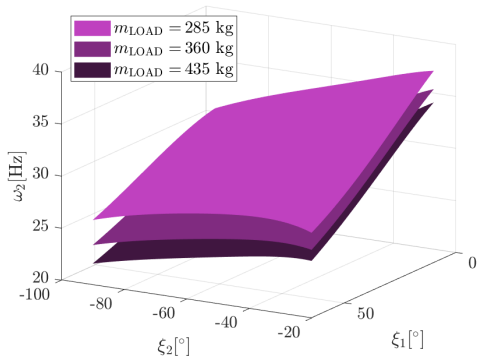

Figure 11 NF ω_2 distribution over the $\xi_1 - \xi_2$ plane (EMLA).

5 Conclusion

The near future is expected to bring an inevitable rise in all-electric heavy-duty manipulator solutions. These solutions will certainly induce new values for a palette of different important manipulator properties. Compared to all-hydraulic solutions, some of these may prove more favourable and will undoubtedly challenge hydraulics in certain aspects.

EMLAs can not outperform hydraulics in many aspects like high-speed actuation with high impact loads like in excavators, of which about 500.000 units are sold annually. Also, challenges regarding cooling are bound to exist in EMLAs, and these will require appropriate analyses.

In any case, addressing differences between hydraulically and electrically actuated manipulators where appropriate transition could occur and making relevant comparisons presents an essential investment to the knowledge base that is bound to gain more and more popularity as time goes by.

In hydraulic solutions, linear actuators are omnipresent, appearing both in prismatic and revolute segments. The same is expected to be encountered in all-electric solutions, leading to EMLAs playing an indispensable role. Since a ballscrew assembly often encountered in precision machining serves as one of the main constituting EMLA subsystems, the already existing and vast body of literature can serve as a foundation for analysis of heavy-duty manipulators with EMLAs.

The main mechanical properties of EMLAs that contribute to the equivalent stiffness are listed and analyzed in a fair amount of detail. Equations of motion for a complex and relevant manipulator arm configuration have

been derived and linearized in the vicinity of a general equilibrium point. Equivalent hydraulic stiffnesses of linear hydraulic and electric actuators have been used in the following analysis to replace the linear actuators with linear springs and calculate the frequencies of natural oscillations of a considered structure.

Based on the obtained results, it is expected that retrofitting EMLAs to existing heavy-duty manipulator arms or creating new all-electric ones will contribute to achieving overall higher values for minimum natural frequencies of manipulator oscillations. Higher values for this crucial structural quality indicator are favourable and could enable better positioning precision and the easier achieving of the higher closed-loop bandwidth. The presented study show that it is expected to achieve up to 3 times higher frequencies of natural oscillations.

Considering manipulator links as rigid bodies, the distribution of natural oscillation frequencies is plotted over the grid of generalized coordinates and will remain to serve as a road sign for future analyses.

References

[1] M. Krefft and J. Hesselbach, "Elastodynamic optimization of parallel kinematics," in *Proc. IEEE Inter. Conf. Autom. Sci. Eng.*, Edmonton, AB, Canada, Aug. 1–2, 2005, pp. 357–362, DOI: 10.1109/COASE.2005.1506795.

[2] J.-P. Merlet, "Jacobian, manipulability, condition number, and accuracy of parallel robots," *Journal of Mechanical Design*, vol. 128, no. 1, pp. 199–206, Jan. 2006, DOI: 10.1115/1.2121740.

[3] D. Liang, Y. Song, T. Sun, and G. Dong, "Optimum design of a novel redundantly actuated parallel manipulator with multiple actuation modes for high kinematic and dynamic performance," *Nonlinear Dynamics*, vol. 83, no. 1, pp. 631–658, Jan. 2016, DOI: 10.1007/s11071-015-2353-1.

[4] T. Sun, B. Lian, Y. Song and L. Feng, "Elastodynamic optimization of a 5-DoF parallel kinematic machine considering parameter uncertainty," *IEEE/ASME transactions on mechatronics*, vol. 24, no. 1, pp. 315–325, Feb. 2019, DOI: 10.1109/TMECH.2019.2891355.

[5] P. Glogowski, M. Rieger, J. B. Sun, and B. Kuhlenkötter, "Natural frequency analysis in the workspace of a six-axis industrial robot using design of experiments," *Advanced Materials Research*, vol. 1140, pp. 345–352, Aug. 2016., DOI: 10.4028/www.scientific.net/AMR.1140.345.

[6] A. Karim, J. Hitzer, A. Lechler, and A. Verl, "Analysis of the dynamic behavior of a six-axis industrial robot within the entire workspace in respect of machining tasks," in *Proc. IEEE Int. Conf. Adv. Intell. Mech. (AIM)*, Munich, Germany, Jul. 3–7, 2017, pp. 670–675, DOI: 10.1109/AIM.2017.8014094.

[7] J. Sun, W. Zhang, and X. Dong, "Natural Frequency Prediction Method for 6R Machining Industrial Robot," *Applied Sciences*, vol. 10, no. 22, art. no. 8138, Nov. 2020., DOI: 10.3390/app10228138.

[8] M. Bottin, S. Cocuzza, Silvio, N. Comand, and A. Doria, "Modeling and identification of an industrial robot with a selective modal approach," *Applied Sciences*, vol. 10, art. no. 4619, Jun. 2020., DOI: 10.3390/app10134619.

[9] A. Doria, S. Cocuzza, Silvio, N. Comand, M. Bottin, and A. Rossi, "Analysis of the compliance properties of an industrial robot with the Mozzi axis approach," *Robotics*, vol. 8, art. no. 80, Sep. 2019., DOI: 10.3390/robotics8030080.

[10] H. N. Huynh, H. Assadi, E. Riviere-Lorphevre, O. Verlinden, and K. Ahmadi, "Modelling the dynamics of industrial robots for milling operations," *Robotics and Computer-Integrated Manufacturing*, vol. 61, art. no. 101852, Jun. 2020., DOI: 10.1016/j.rcim.2019.101852.

[11] B. Lian, L. Wang, and X. V. Wang, "Elastodynamic modeling and parameter sensitivity analysis of a parallel manipulator with articulated traveling plate," *The International Journal of Advanced Manufacturing Technology*, vol. 102, no. 5, pp. 1583–1599, Jan. 2019., DOI: 10.1007/s00170-018-03257-x.

[12] J. Kovanen and H. Handroos, "Adaptive open-loop control method for a hydraulically driven flexible manipulator," in *Proc. IEEE/ASME Inter. Conf. Adv. Intell. Mech.*, Como, Italy, Jul. 8–12, 2001, pp. 942–947, DOI: 10.1109/AIM.2001.936805.

[13] L. Zhai, T. Virvalo, J. Mattila, and H. Saarinen, "Analysis and control of a water hydraulic manipulator for ITER divertor remote maintenance," *International Journal of Fluid Power*, vol. 11, no. 1, 2010., DOI: 10.1080/14399776.2010.10780997.

[14] M. Rigotti-Thompson, M. Torres-Torriti, F. A. Cheein, and G. Troni, "$\mathcal{H}_\infty$-Based Terrain Disturbance Rejection for Hydraulically Actuated Mobile Manipulators With a Nonrigid Link," *IEEE/ASME Transactions on Mechatronics*, vol. 25, no. 5, pp. 2523–2533, Oct. 2020., DOI: 10.1109/TMECH.2020.2983072.

[15] D. Vandenbroucke, A. Van Hyfte, and L. Francx, "Study in View of the Revision of Directive 97/68/EC on Non-Road Mobile Machinery (NRMM)," An Emissions Inventory and Impact Assessment, Final Report, 2010. [Online]. Available: https://op.europa.eu/s/vUdn

[16] G. Qiao, G. Liu, Z. Shi, Y. Wang, S. Ma, and T. C. Lim, "A review of electromechanical actuators for More/All Electric aircraft systems," *Proceedings of the Institution of Mechanical Engineers, Part C: Journal of Mechanical Engineering Science*, vol. 232, no. 22, pp. 4128–4151, 2018., DOI: 10.1177/0954406217749869.

[17] G. R. Petrović and J. Mattila, "Mathematical modelling and virtual decomposition control of heavy-duty parallel–serial hydraulic manipulators," *Mechanism and Machine Theory*, vol. 170, Art. no. 104680, pp. 1–26, Jan. 2022, DOI: 10.1016/j.mechmachtheory.2021.104680

[18] A. Cibicik and O. Egeland, "Dynamic modelling and force analysis of a knuckle boom crane using screw theory," *Mechanism and Machine Theory*, vol. 133, pp. 179–194, Mar. 2019., DOI: 10.1016/j.mechmachtheory.2018.10.019.

[19] R. Jazar, "Motion Dynamics," in *Theory of applied robotics: kinematics, dynamics, and control*, 2nd ed., New York, NY, USA: Springer, 2010, ch. 11, sec. 1–8, pp. 581–628, DOI: 10.1007/978-1-4419-1750-8

[20] W. H. Zhu, *Virtual decomposition control: toward hyper degrees of freedom robots*, 1st ed., Berlin Heidelberg: Springer-Verlag, 2010, DOI: 10.1007/978-3-642-10724-5

[21] G. R. Petrović and J. Mattila, "Analytic Solutions for Wheeled Mobile Manipulator Supporting Forces," *arXiv preprint arXiv:2202.10186*, Feb. 2022., DOI: 10.48550/arXiv.2202.10186

[22] L. Meirovitch, "Nonconservative systems. The nonsymmetric eigenvalue problem.," in *Principles and techniques of vibrations*, 1st ed., New Jersey, NJ, USA: Prentice Hall, 1997, ch. 4, sec. 8, pp. 189–195

[23] H. E. Merritt, "Valve controlled piston.," in *Hydraulic control systems*, John Wiley and Sons, 1967, ch. 6, sec. 2, pp. 145–150

[24] S. Frey, A. Dadalau, and A. Verl, "Expedient modeling of ball screw feed drives," *Production Engineering*, vol. 6, no. 2, pp. 205–211, Apr. 2012, DOI: 10.1007/s11740-012-0371-0

[25] I. Ansoategui, and F. J. Campa, "Mechatronics of a ball screw drive using an N degrees of freedom dynamic model," *The International Journal of Advanced Manufacturing Technology*, vol. 93, no. 1, pp. 1307–1318, Jun. 2017, DOI: 10.1007/s00170-017-0597-2

[26] R. Caracciolo and D. Richiedei, "Optimal design of ball-screw driven servomechanisms through an integrated mechatronic approach," *Mechatronics*, vol. 24, no. 7, pp. 819–832, Oct. 2014, DOI: 10.1016/j.mechatronics.2014.01.004

[27] M. S. Kim and S. C. Chung, "Integrated design methodology of ball-screw driven servomechanisms with discrete controllers. Part I: Modelling and performance analysis," *Mechatronics*, vol. 16, no. 8, pp. 491–502, Oct. 2006, DOI: 10.1016/j.mechatronics.2006.01.008